Journal of Applied Fluid Mechanics, Vol. 18, No. 2, pp. 504-517, 2025.
Available online at www.jafmonline.net, ISSN 1735-3572, EISSN 1735-3645.
https://doi.org/10.47176/jafm.18.2.2769

Aerodynamic Optimization of 3D Micro HAWT Blade via RSM

R. Bekkai, R. Mdouki† and R. Laouar

Laboratory of Environment, Faculty of Sciences and Technology, Echahid Cheikh Larbi Tebessi University, Tebessa, 12002, Algeria

†*Corresponding Author Email: ramzi.mdouki@univ-tebessa.dz*

ABSTRACT

The goal of this research is to redesign the three-dimensional geometry of a micro horizontal-axis wind turbine blade using response surface methodology. The variation of the two influential design parameters, chord length and twist angle, along the blade is geometrically modelled using a fourth- and second-degree polynomial, respectively. Therefore, the optimization process is performed basing on eight input parameters that describe the initial blade design. The performance of the initial and the new optimized wind turbine are compared using CFD and BEM approaches. To well study fluid flow through the wind turbine and assess its performance, the CFD analysis step is carried out using the RANS equations with the k-ω SST turbulence model. Concerning the optimization step, The MOGA (Multi-Objective-Genetic Algorithm) method is employed in an automated manner based on a metamodel with non-parametric regression NPR to identify the best candidate with high efficiency. The performance of turbine rotor types is analyzed using the open source Qblade software and compared with CFD methodology for different TSR (Tip Speed Ratio) values. An increase of 14.65% and 17.17% in power coefficient is marked for CFD and Qblade, respectively, at the design TSR of 3. Compared to the initial blade, the optimal one produces more lift, has a lower separation area, and performs significantly better performance at all TSR values. The detailed representation of 3D flow via pressure distribution and limiting streamlines on both blade surfaces confirm the optimization target which leads to reduce separation zones and improve rotor torque. Additionally, a 37% improvement in starting operability at the lowest wind speed is achieved compared to the initial rotor.

Article History

Received April 8, 2024
Revised September 5, 2024
Accepted September 17, 2024
Available online December 4, 2024

Keywords:

CFD
MOGA
RANS
Response Surface Method
Qblade
Optimization

1. INTRODUCTION

Although changes in political and social conditions have boosted renewable energy growth in recent decades, the current energy system is primarily reliant on fossil fuels. In fact, wind source is an important renewable energy with its vast reserves over the entire terrestrial globe and it is still far from reaching its full potential. Therefore, the use of wind turbines necessities aerodynamic design to extract optimal wind power. In this context, numerous works of literature have used the blade element momentum approach, which was established originally for Aeroplan propellers (Glauert, 1976), for the design and performance computation of the blades. To assess wind turbine performance, both momentum and blade element theories are coupled. Using these theories, several researchers have predicted Wind turbine performance (Ceyhan et al., 2009; Kim et al., 2011, 2013; Reddy et al., 2019; Sessarego et al., 2020; Tahani and Moradi, 2016).

Furthermore, the CFD analysis with a suitable turbulence model is one of the most extensively used methodologies for evaluating wind turbine performance. Pape and Lecanu (2004) used the k - ω SST turbulence model to evaluate the aerodynamic performance of a NREL wind turbine, and the results are in good agreement with the experiment results at low speeds. Lanzafame et al. (2013) created a 3D CFD model to predict the performance of a micro HAWT and assess the capabilities of the 1D BEM model. Using NREL PHASE 4 experimental data, two turbulence models, two equations SST k-ω fully turbulent and four equations transitional SST models, were employed, compared, and verified. The difference between simulated and experimental results was less than 6%. To enhance the blade root region and increase the efficiency of the wind turbine, (Bai et al., 2016) proposed a mathematical model to evaluate the lift and drag coefficient for different airfoil profiles. A comparative analysis between both approaches CFD and BEM was carried out. Using k-ω SST turbulence model,

Nomenclature

P	output power	σ	solidity
V	wind speed	φ	inflow angle
B	number of blades	λ_r	local tip speed ratio
C_p	power coefficient	β	twist angle
C_L	lift coefficient	RSM	Response Surface Method
C_D	drag coefficient	CCD	Centre Composite Design
C_L/C_D	glide ratio	DOE	Design Of Experiment
C	chord length	TSR	Tip Speed Ratio
C_n	normal force coefficient	HAWT	Horizontal Axis Wind Turbine
C_t	tangential force coefficient	VAWT	Vertical Axis Wind Turbine
Htr	hub tip ratio	MOGA	Multi-Objective -Genetic Algorithm
Q	torque	RANS	Reynolds Averaged Naiver Stokes
ω	rotational speed	MRF	Moving Reference Frame Model
α_D	design angle of attack	R^2	coefficient of correlation

a good agreement between the two methods was found. Rajib et al. (2019) presented a numerical study with CFD and Qblade software to explore the performance of mixed airfoil small scale horizontal axis wind turbine blades. After selecting two airfoil profiles SG 6040 and SG 6043 at the root and tip region, respectively, the obtained results using the k- ω SST turbulent model in the CFD tool show a good performance. Casillas et al. (2022) proposed a new prototype of the induction blade (IB) which was designed using BEM theory. The CFD analyzer was also used to evaluate the aerodynamic properties with the turbulent model k-ω SST. The studied (IB) model provides 65% extra torque compared with a conventional blade which was designed using BEM theory. In the field of enhancing blade efficiency, most of the previous works have concentrated on passive aerodynamic optimization based on the classical approach which leads to an optimal blade design through a series of iterations with high cost in term of time and computational resources. In the modern methods, the optimization requires a simple design scheme with many design parameters to obtain an optimum aerodynamic design at an early stage of the design process, as well as to correlate significant design factors. One of these modern methods is the response surface methodology (RSM) which represents a statistical technique used to investigate the relationship between numerous design variables and one or more response variables. Benim et al. (2018) optimized an airfoil profile for a small horizontal-axis wind turbine using RSM methodology based on computational fluid dynamics with Biobjective Mesh Adaptive Direct Search Optimization algorithm (BMADSO). The results demonstrated that this procedure can be an effective tool for optimizing the shape of the blade. Sun (2011) proposed a parametric study to investigate the effect of design factors with varying nominal angles of attack and assess the airfoil performance. Therefore, the response surface method (RSM) was used to find the best design based on the objective functions (minimum drag coefficient or a maximum lift-to-drag ratio) and constrains (the lift coefficient of a designed airfoil is higher than that of a base airfoil at a certain angle of attack). It was found that the RSM methodology can be effective for improving the aerodynamic characteristics of wind turbine airfoils. In The study of (Tabatabaeikia et al., 2016), the response surface approach was employed to enhance statistical procedures. The generated power coefficient is used as an objective function in the optimization process. The turbulence phenomena were modelled with the k-ω SST, and the simulation results were validated with experimental data, which revealed a small variation of less than 9 %. It also showed that the optimization method led to a 48.8 % increase in wind turbine power compared to the initial design. Hung et al. (2016) proposed a design for a counter-rotating horizontal axis tidal turbine (HATT) using BEM method which fails to forecast the interaction between the two rotors. CFD tool was used to compensate this BEM failure. A second order RSM was utilized to identify the best setting angles for both front and rear rotor blades. Wind tunnel test was conducted to validate the CFD results. The numerical model was validated via wind tunnel measurements. The optimal configuration leads to a high performance for all TSRs. Li et al. (2010) applied an aerodynamic optimization strategy for 2-D wind turbine airfoil which is based on a combination of RSM method and uniform experimental design. This technique maximizes the airfoil lift-to-drag ratio at the design angle of attack. Another approach, used in the optimization field, tries to discover combinations of the main design parameters, and find the best one. This approach become a robust tool to reach the optimization goal with high accuracy and short computational time. Lee and Shin (2020) used combined input parameters methodology for designing wind turbine blades with a maximum efficiency increase of 8% using a second order RSM coupled with BEM on Minitab software. Zhou et al. (2020) studied the performance of the Inertia Particle Separator (IPS), which has been enhanced using the interaction between input parameters through RSM method. The IPS separation efficiency on AC-Coarse dust is increased by 3.8%. In the research paper of (Aelaei et al., 2019), the effect of mixing input parameters on delta wing performance was explored using optimization technique NSGA-II (Non-dominated Sorted Genetic Algorithm-II) coupling with the RSM method. Based on the CFD analyzer and the optimization methodology, the aerodynamic efficiency was increased by 50% compared to the initial wing. Therefore, the highest angle of attack at Mach number 1.2 was chosen as the best design point for the vehicle. Dual-rotor wind turbine was studied by Taghinezhad et al. (2021) to improve its performance using the RSM methodology. The different operating conditions extracted for this type

of turbine were also compared and the results showed a maximum power ratio of about 55% in the optimal conditions. Moreover, the power ratio of the studied model agreed well with the experimental data. The objective of the work conducted by Akhlaghi et al. (2023) was to investigate the effect of each design parameter on the performance and self-starting ability of the Darries VAHT. Therefore, using Kringing optimization method leads to obtain optimum configuration with a blended input parameters strategy. In additionally relying on RSM methodology 10% increase in performance at optimal TSR was obtained.

Despite the high accuracy offered by the deep learning approach, the former requires extensive training data, which raises; costs and defeats the purpose of optimization. This shortcoming, the deep learning method could be avoided by selecting the robust surrogate model to achieve an optimal design. Several studies have been proposed to support the advantages of using the surrogate model. Yang et al. (2023) proposed an improved Gaussian process regression (GPR) model, adding an enhanced kernel construction algorithm (AKC), for the accurate prediction of dynamic parameters. The combined model AKC-GPR shown exceptional accuracy, establishing itself as a reliable and robust surrogate for predictive modeling. Yang et al. (2024a) introduced a robust method coupling proper orthogonal decomposition (POD) with a surrogate model via the AKC-GPR algorithm. This approach enhances the aerodynamic configuration of UAV-BWB vehicle by reducing geometric parameters. Consequently, CFD results demonstrated a 14 % increase in the lift-to-drag ratio for the optimal design compared to the initial one. Yang et al. (2024b) implemented a reduced- order model (ROM) for quick 3D hypersonic vehicle flow. With this enhanced model AKC-GPR, a reduction of 35.28 % in the mean absolute percentage error (MAPE) was compared the baseline model.

In the present study, an investigation based on an optimization procedure was performed to improve the performance of micro wind turbine using the RSM methodology based on CFD Analyzer and Qblade Software. A metamodel with non-parametric regression NPR coupling with the MOGA method was used to provide an enhanced response. In this regard, the input parameters were chosen with high efficiency to describe both chord length and twist angle distribution along the blade through polynomial functions with eight parameters based on the initial blade geometry. Compared to the previous research work (Bekkai et al., 2024), experimental data was added to confirm the accuracy of numerical approach with selecting the powerful polyhedral mesh type and using the best aerodynamic profile SG 6043. Furthermore, the torque assessment at different speeds leads to an improvement in the starting operate ability at the lowest wind speed compared to the initial rotor.

2. WIND TURBINE BLADE DESCRIPTION

2.1 Aerodynamic Characteristics Analysis of Airfoil

The SG6043 is an element of the SG604x airfoil family, which is well known for its outstanding aerodynamic characteristics at low Reynolds numbers (Shin & Kim, 2020). Figure 1 shows the airfoil profile. The relative geometric proprieties of the airfoil section; maximum thickness, camber and leading-edge radius have the following values 10%, 5.5% and 1.7%, respectively. The glide ratio Cl/Cd variation with respect to the angle of attack of the SG6043 airfoil at Re=4×10^4 is illustrated in Fig. 2. In this part, the open 2D software Xfoil is used to calculate the aerodynamic properties of the airfoil (Drela, 2001). Therefore, the obtained ranges of the glide ratio and the angle of attack are limited between [0, 5] and [-1, 16], respectively, with the design value of the angle of attack equals to 10°.

2.2 Blade Design

The initial turbine rotor is identified with blades number B=3, rotor diameter D=0.6m, hub tip ratio htr=0.1, and design tip speed ratio TSR=3. Using the Schmitz approach (Marten & Wendler, 2013), the wind turbine blade design is determined by the distribution of both chord length and twist angle along the blade span, as shown in the following equations:

$$\beta = \frac{2}{3} tan^{-1}\left(\frac{1}{\lambda_r}\right) - \alpha_D \quad (1)$$

$$C = \frac{16\pi r}{BC_L}\left(\sin\left(\frac{1}{3}\tan^{-1}\frac{1}{\lambda_r}\right)\right)^2 \quad (2)$$

In the analysis step, the Blade Element Momentum method (BEM) in which two theories are blended: momentum theory and blade element theory, is employed. This method concerns with the responsible force for producing rotor motion through fluid flow. The Wind

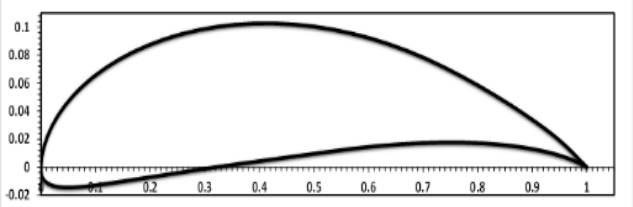

Fig. 1 Airfoil section shape for SG6043

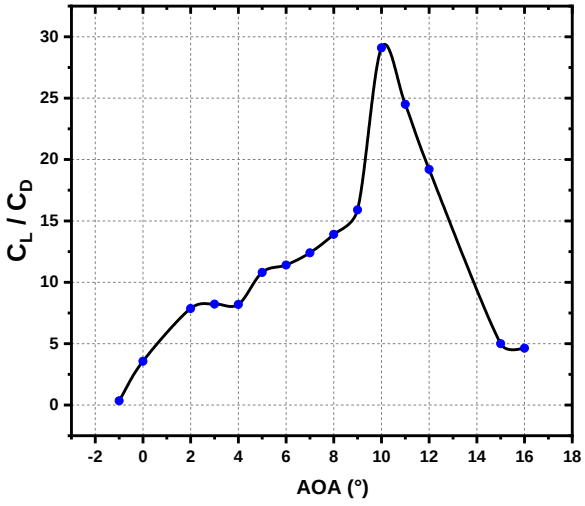

Fig. 2 Aerodynamic Characteristics of SG6043 at Re=4×10^4

turbine blade is divided into small blade sections, and the conservation of linear and angular momentum was applied to all segments of the blade, resulting in the calculation of forces and power. The induction factors and airfoil aerodynamic characteristics are the two main keys in BEM theory. This latter (Marten & Wendler, 2013) was analyzed using the open-source Software Qblade, where the entire blade is divided into 40 small elements. The lift and drag coefficients are calculated for each element of the blade iteratively until the induction factors are expected to converge (Sørensen, 2016). The axial and tangential induction factors are defined as follows:

$$a = \left(\frac{4\sin^2\varphi}{\sigma C_N} + 1\right)^{-1} \quad (3)$$

$$a' = \left(\frac{4\sin\varphi\cos\varphi}{\sigma C_t} - 1\right)^{-1} \quad (4)$$

where φ denotes the inflow angle and Cn and Ct denote the tangential and normal force coefficients, respectively. The rotor solidity σ is defined by:

$$\sigma = \frac{cB}{2\pi r} \quad (5)$$

Where c, B and r represent the chord length, blade number, and radial positions of the turbine blade (Hasan et al., 2017). In this study, the maximum number of iterations was set at 100. After convergence, the associated parameters are used to calculate the generated power for that specific blade element and this procedure was repeated for all blade sections. Several correction models, such as, new tip loss, new root loss, 3d correction, Reynolds drag correction, and airfoil interpolation, were also used in BEM to ensure its accuracy.

3. GEOMETRY PARAMETRIZATION

After selecting the optimal tip speed ratio of TSR=3, and wind speed of 6 m/s, the distribution of chord length and twist angle for initial blade design can be extracted. To represent the changes in chord length and twist angle, a fitting curve was applied with high efficiency to match the initial design. Therefore. Both distributions of chord length and twist angle are developed by fourth degree and quadratic polynomial fitting, respectively (Zach, 2021), as shown in the following equations:

$$C(r) = a_1.r^4 + a_2.r^3 + a_3.r^2 + a_4.r + a_5 \quad (6)$$

$$\beta(r) = b_1.r^2 + b_2.r + b_3 \quad (7)$$

Where r is the radial position along the blade, a_1, a_2, a_3, a_4, and a_5 are coefficients that represent variation in chord length along the blade, whereas b_1, b_2, and b_3 are coefficients related to the change in twist angle on the blade. Figure (3,4). Shows the chord length and twist angle distributions after the fitting procedure.

4. COMPUTATIONAL FLUID DYNAMICS (CFD)

The studied configuration is based on the geometric proprieties summarized in Table 1 with wind speed of 6 m/s, tip speed ratio of 3 and number of blades B=3. Following the main steps of the CFD procedure, the geometry construction, grid generation, and governing equation solving, are illustrated in the following paragraphs.

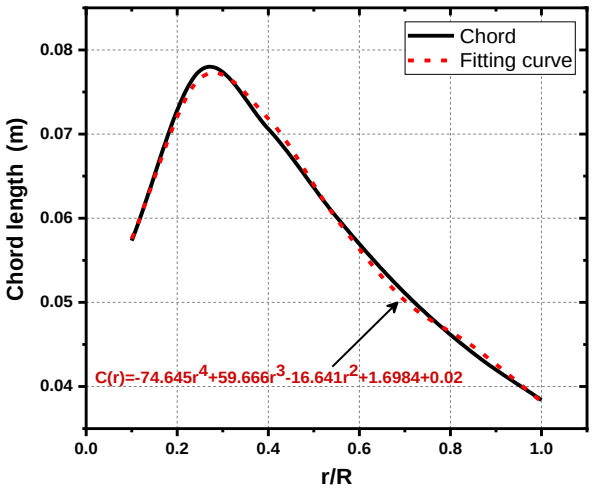

Fig. 3 chord length distribution with fitting curve

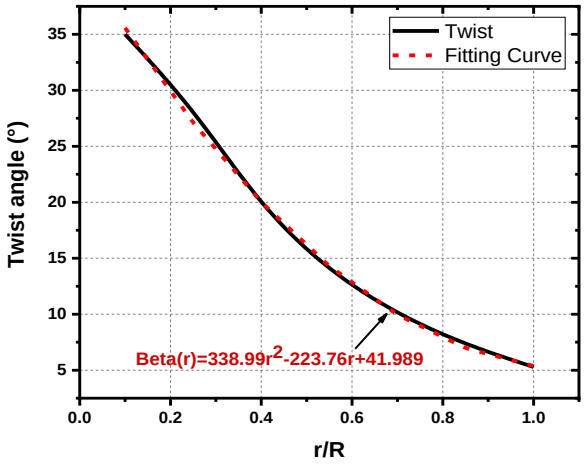

Fig. 4 Twist angle distribution with fitting curve

Table 1 Geometry specification of fluid domain with blade

Geometric Specification	Value
Blade Radius	0.3 m
Hub Radius	0.03 m
Inlet velocity Radius	3 m
Exit velocity Radius	6 m

4.1 The Geometry of the Fluid Domain with the Blade

The geometry domain is represented by a truncated cone with an inlet at the small base and an outlet at a big base. To minimize the number of cells simulation, a third of the domain including one blade is considered, Fig. 5. The blade is located inside the domain, with both upstream and downstream distances equal to 10 and 20 times the rotor radius to predict the relevant phenomena such as the wake region (Hasan et al.,2017).

Table 2 Mesh - Independency

Element size on the blade surface (m)	Number of cells (polyhedral)	Torque value (N.m)	Performance of Turbine
0.0005	2.7 million	0.081	0.38
0.0008	1.1 million	0.08005	0.38
0.001	0.86 million	0.08	0.38
0.0015	0.8 million	0.07	0.37

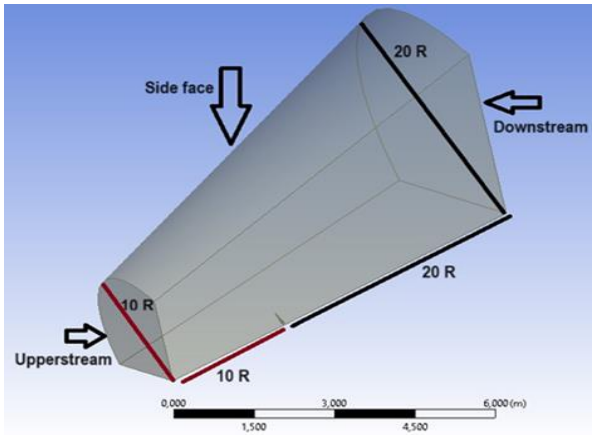

Fig. 5 Illustration of the fluid domain

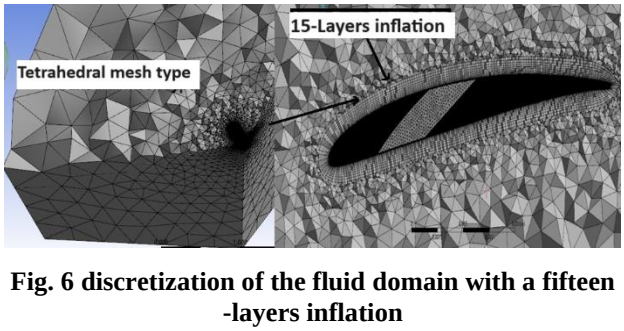

Fig. 6 discretization of the fluid domain with a fifteen -layers inflation

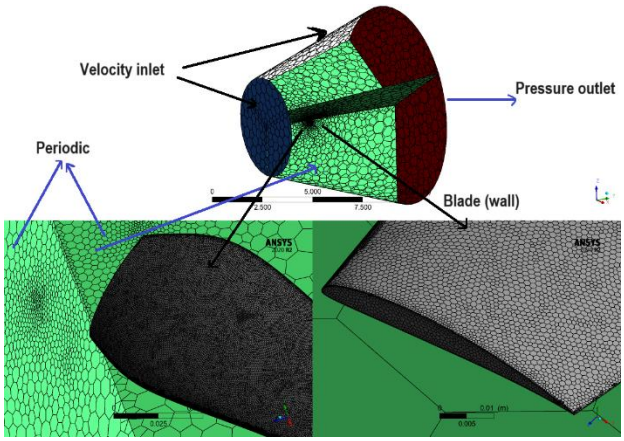

Fig. 7 discretization of the blade domain and boundary condition

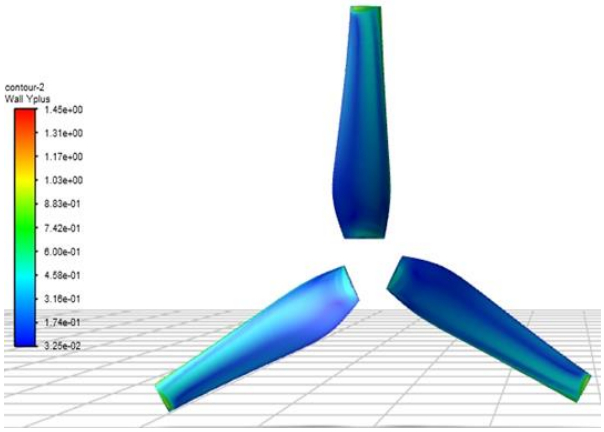

Fig. 8 y+ distribution around the blades

4.2 Computation Grid

The constructed geometric domain is discretization using two kinds of meshes: polyhedral and tetrahedral, Fig (6 and 7). The former is used to improve the latter in both accuracy and number of cells (Mauro et al., 2017). The grid solution independence is carried out to choose the most convenient mesh. Therefore, in Table 2, the output results reach a constant value of 0.38 and 0.08 for the mesh identified by 0.86 million cells. Moreover, a 15-layer inflation was also formed near the blade wall, with a calculated y+ on the blade surface of less than 10 (Koç et al., 2016). With a growth rate of 1.2, the height of the first neighboring wall cells is almost 1.410^{-5} m which is estimated using the y+ calculator website with the following formula:

$$y+ = w\,\Delta y\,\rho / \mu \quad (8)$$

Where w, Δy, ρ and μ are relative velocity, the thickness of the first layer, air density and dynamic viscosity, respectively.

Figure 8 also shows the distribution of y+ around the blades for the selected mesh. The maximum value of y+ equals 1.45 in the tip region, it can be also noted that the leading and trailing edges of the blade maintain a value of y+ close to 1.

4.3 CFD Solver and Boundary Conditions

The commercial software Ansys-Fluent is the CFD tool based on the finite volume method and is used in this work to model numerically the wind turbine aerodynamic performance. The Shear-Stress Transport (SST) k-ω turbulent model for the Reynolds-averaged Navier-Stokes (RANS) equations were employed in the CFD investigation. The SST turbulence model combines and includes a smooth transition between the k-ε and k-ω turbulence models; k- ω delivers better compromises near the wall, while k- ε provides a better solution in the bulk domain (Menter et al., 2003). In addition, second-order upwind discretization was applied in space. During the

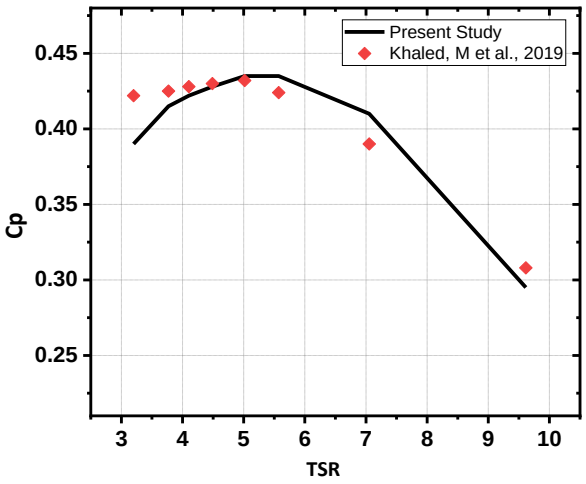

Fig. 9 Validation with the literature review at the wind speed of V=6 m/s

iterative process, the convergence rate was determined using the residuals of the dependent variable of the governing differential equations with 10^{-5} of accuracy.

The boundary conditions for the domain are defined as "velocity inlet "at the small base and lateral face of the cone. The "pressure outlet" is defined at the big cone base. Whereas the remained faces are considered as periodic as seen in Fig. 7. Moreover, the Moving Reference Frame Model (MRF) was employed to provide blade rotation by selecting angular velocity ω =60 rad/s.

4.4 Numerical Approach Validation

To validation the numerical approach with experimental data, the results in the work of (Khaled, et al., 2019) were used. This analysis was conducted using a wind turbine rotor with a diameter of 0.7m at design wind speed of 6m/s. three blades and hub tip ratio of 10% identify the rotor. The aerodynamic blade geometry is characterized by NACA 4412 airfoil section with chord length and twist angle varied from 0.003 m and 1.7° at blade tip to 0.068 m and 36.44° at blade root, respectively.

The rotor was tested in a low speed wind tunnel facility at Ain Shams University in Egypt. This validation is carried out maintaining the same flow domain dimension and the same mesh characteristics with a skewness factor less than 0.85 and k-ω SST turbulent model. Comparison between both numerical and experimental results shows a good agreement and leads to a well reliability permitting the using of the numerical approach, Fig 9. The peak power coefficient is predicted numerically at TSR=5 with almost the value of 0.435, while it is equal 0.432 experimentally.

To estimate numerical results accuracy, the correlation coefficient R^2 is examined through the following statistical equations (Maindonald, and Braun 2010):

$$R^2 = 1 - \frac{\Sigma(\varphi_{exp} - \varphi_{pred})^2}{\Sigma\left(\varphi_{exp} - \varphi_{exp}^{avg}\right)^2} \quad (9)$$

Where:

$$\varphi_{exp}^{avg} = \left(\sum_{i=1}^{n} \varphi_{exp}\right) / n \quad (10)$$

After achieving the correlation coefficient $R^2 = 0.85$ at the same CFD parameters used in this study, a good convergence between the two approaches results can be proven. This allows that the current numerical approach can be adopted for all simulations with high accuracy.

5. GOAL DRIVEN OPTIMIZATION

The design optimization process is based on the following three steps:

5.1 Design of Experiment (DOE)

In this step, a test sample of input parameters is generated to cover the whole range of these parameters with a minimum number of design points. The effect of the input parameters on the output ones is revealed by keeping the test samples with high efficiency. Moreover, the constraints on each input parameter are extended by 20% for upper and down values, Table 3. The DOE technique aims to identify sampling sites in the design space in such a way that the space of random input parameters is explored in the most efficient manner obtaining the required response with the minimum possible sampling points (Design Xplorer Documentation, 2010).

Following the development of the test sample in the DOE table, the Central Composite Design (CCD) method is utilized with a four-level sampling design. The optimizer then repeats all the operations done in the initial design (drawing, meshing, solving governing equations and estimating output parameters) for all design points in the DOE table. The preliminary design has been created in this investigation and provides a parallel chart of parameters for 38 sample points with input parameters, Fig. 10.

Table 3 Constraints used in the optimization process

Input parameters constraints	Chord constraints (m)	Twist constraints (°)
-89.57≤a1≤-59.71	-	-
47.7≤a2≤71.6	0.03≤C1≤0.08	20≤ β1≤44
-19.97≤a3≤-13.3	0.042≤C2≤0.115	17≤ β2≤35
3.057≤a4≤1.358	0.04≤C3≤0.115	10≤ β3≤32
0.016≤a5≤0.024	0.035≤C4≤0.11	5≤ β4≤25
271.192≤b1≤406.788	0.025≤C5≤0.096	3≤ β5≤20
-265.5≤b2≤-179	0.02≤C6≤0.095	1≤ β6≤13
33.6≤b3≤50.388	0.01≤C7≤0.09	-3≤ β7≤10

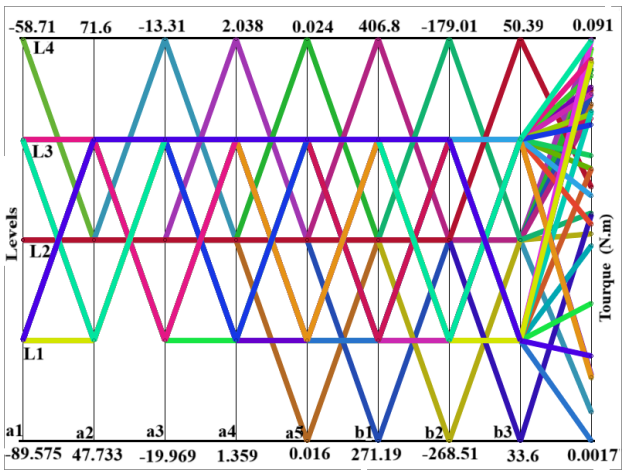

Fig. 10 Parallel diagram

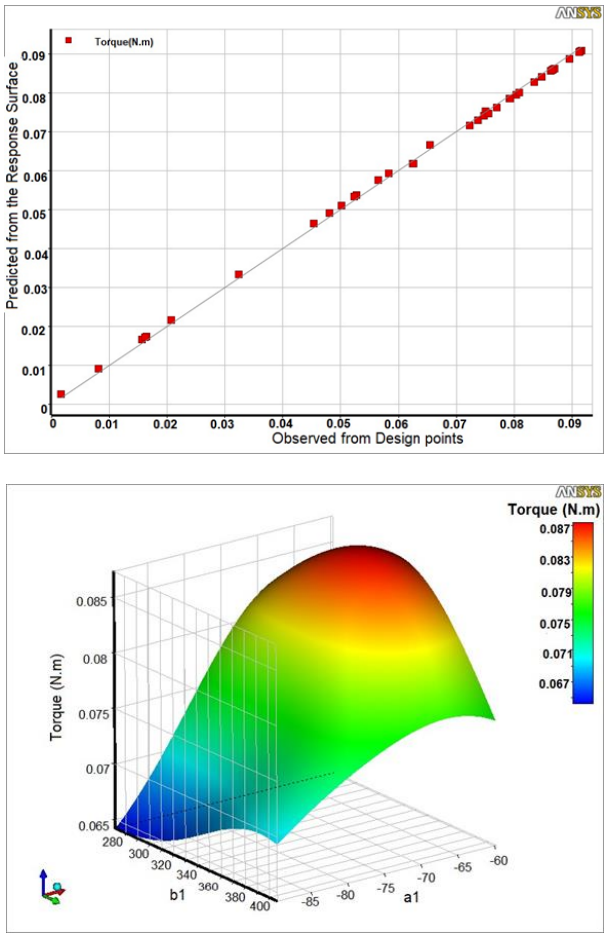

Fig. 11 goodness-of-fit of the response surface using non-parametric regression and the response surface of (a1), (b1) on the torque value

5.2 Response Surface

In this step, the obtained results from the DOE table are used to create a multidimensional correlation which will be used to forecast the system response to change the input parameters. A metamodel with non-parametric regression was used to generate the response surface (Design Xplorer Documentation, 2010). This model leads to increased response quality and over predicts the

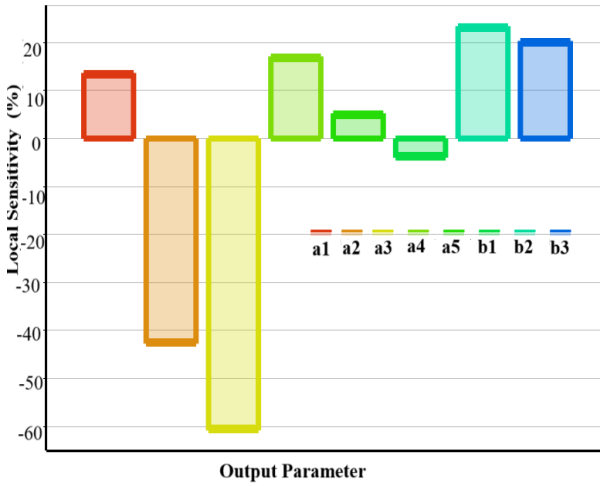

Fig. 12 Local sensitivity of the design parameters for the torque

nonlinear behavior of the goal functions regarding the design parameters. The goodness-of-fit test was used to examine the quality of the response surface based on simulation values. It should be stated that the response surface was produced with great accuracy due to the well-fitted design points related to the value coefficient of determination R^2=0.998, as illustrated in Fig. 11. The influence of each design parameter on the objective function was also investigated using the local sensitivity chart. Figure 12 shows that each input parameter affects the output torque with different values. It should be noticed that the most influential input parameters are a_2, a_3 and b_2, b_3 in both chord and twist expressions, respectively.

5.3 Optimization

With the aim to identify the maximum torque value from the obtained response surface, a new sample set of 8000 points is produced in Goal-driven optimization process based on The MOGA (Multi- Objective- Genetic Algorithm) method. The candidate point with the highest torque value is then chosen for optimal chord length and twist angle distributions using the best input parameters (Table 4).

The optimum design candidate is then validated in the CFD analysis process (ANSYS FLUENT User's Guide, 2010). The detailed optimization steps are illustrated in Fig. 13.

Table 4 Optimum input parameters

Input Parameters	Optimum input parameters
a1	-65.562
a2	54.498
a3	-16.605
a4	1.9704
a5	0.0208
b1	331.69
b2	225.07
b3	39.812

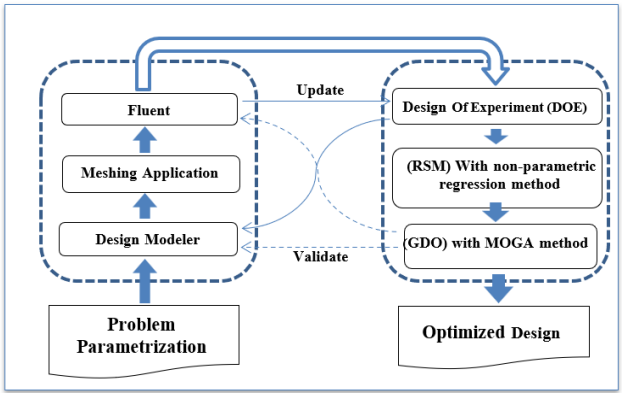

Fig. 13 Design Exploration Algorithm

Table 5 Optimum distribution for both chord and twist

Position (m)	Chord Length (m)	Twist Angle (°)
0.03	0.0663	33.35
0.075	0.096	24.79
0.12	0.098	17.57
0.165	0.090	11.7
0.21	0.079	7.17
0.255	0.0699	3.98
0.3	0.057	2.14

6. RESULT AND DISCUSSION

6.1 Blade Optimization Targets

From Table (4,5), the best chord and twist are derived from the optimal input parameters in the current results for the new blade. In Fig. 14 and Fig.15, the chord length and twist angle distribution are represented in the span-wise direction on the blade and a comparison is carried out with a 3-D view of HAWTs between optimal and initial design. From qualitative of point view, both the initial and optimal blade have almost the same geometry; the chord is large at the root and narrow at the tip and the blade twisting between tip and root maintains the same level. From quantitative point of view, the optimal blade design chord length is higher than the initial one and the twist angle changes weakly between both configurations.

6.2 Pressure Distribution

In the current study, the relative chord length along the initial blade is proposed as a reference which allows us to examine the evolution of the enhanced blade chord length distribution, Fig.16. Based on the static pressure distribution results along the blade, the increase in lift production on the optimal blade at the station near the root region, r/R= 0.20, appears clearly over the entire profile. However, the improvement in lift reveals beyond 20% of the relative chord in the two sections r/R=0.50 and r/R=0.75, with a little drop at the leading edge. On the last section near the tip with r/R = 0.9, an increase in lift production starts almost from the middle profile; 45% of the chord length. It can be noticed that the pressure distribution on the suction side is responsible for the lift improvement on the optimal blade and the increasing of the chord length in all stations compared to the reference

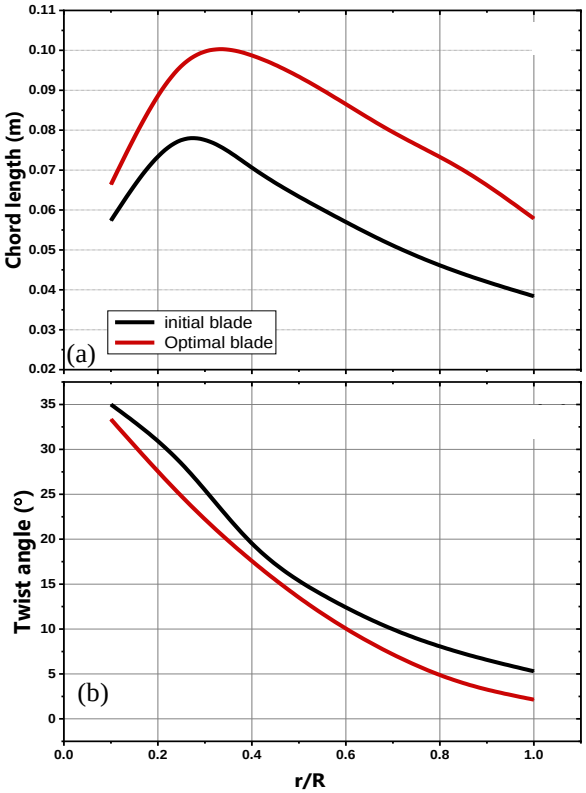

Fig. 14 Comparison between optimal and initial blades, (a) chord length, (b) twist angle

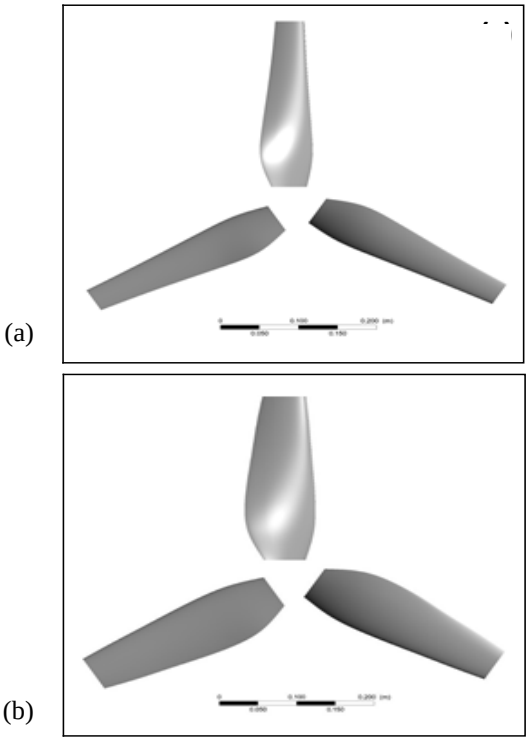

Fig. 15 Comparison of 3D views between optimal and initial wind turbines

length participates in delaying the flow separation on the improved blade. The obtained results confirm the previous discussion related to Fig. 14; the increase in the chord length on the optimal blade leads to an increase in the torque value.

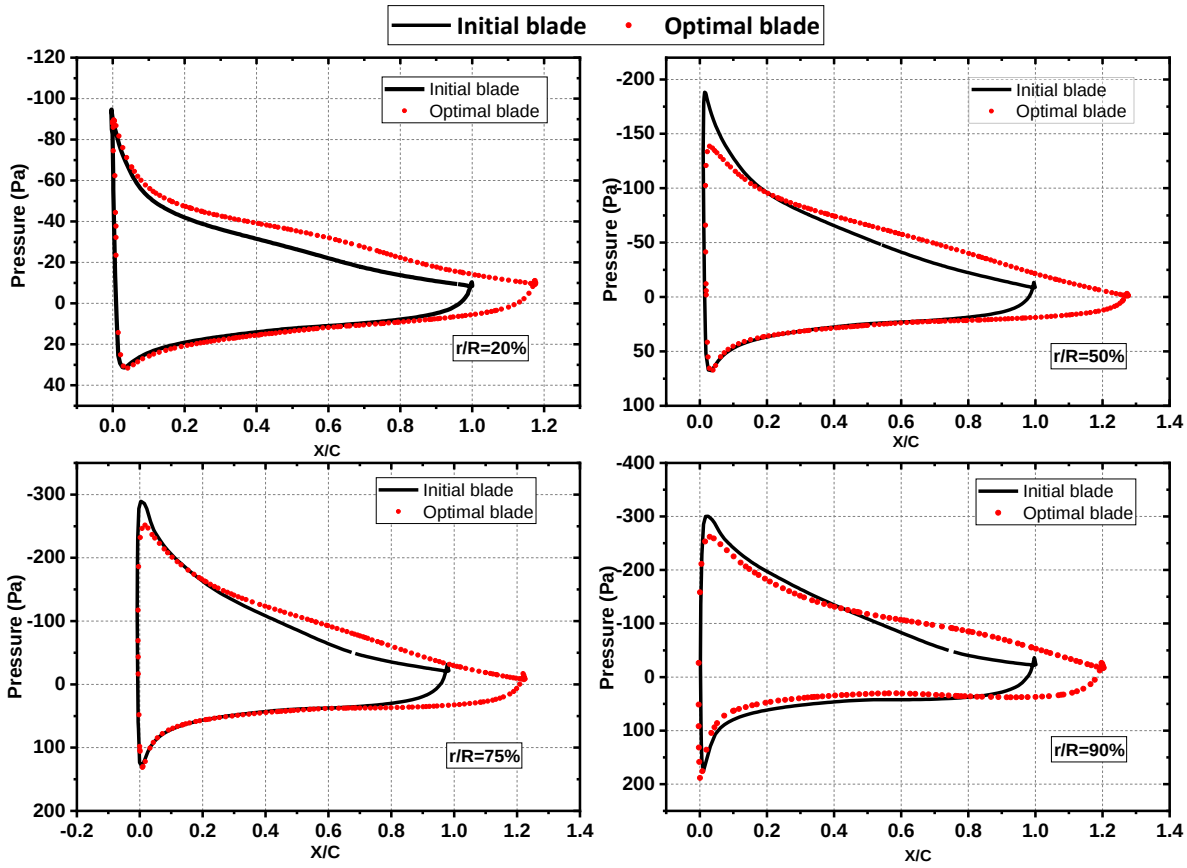

Fig. 16 Pressure distribution comparison between the initial and optimal blade at TSR=3

6.3 Flow Visualization

Figure 17 compares velocity contours and streamlines of the initial and optimal blades at the stations r/R=20, 50, 75, and 90% in the blade span-wise direction at TSR=3 and wind speed of 6 m/s. Separation flow can be observed along the trailing edge when the angle of attack is close to 10° which represents the design configuration with a maximum glide ratio of the SG 6043 airfoil at a Reynolds number of 40.000; based on the maximum chord length. The aerodynamic optimization leads to a delay in the boundary layer separation zone over the suction side near the trailing edge. It is obvious that, in initial blade, the SST turbulent model over-predicted the boundary layer separation at trailing edge. To manipulate this separation, the design angle of attack α_D, should be decreased, therefore, the characteristic curve Cl/Cd vs AoA must be shifted to the left. This case corresponds to increasing the Reynolds number via chord length. Based on velocity triangles, the design angle of attack α_D decreases with the increasing of the chord length. Finally, this confirms the optimization effect; the power coefficient is improved with increasing of the chord length and decreasing of the twist angle. Moreover, it can be observed that local velocity increases from the hub to the tip region for both blades, which agrees with physical phenomena.

Figure 18 represents the development of the limiting streamlines with static pressure contours for both blade sides to difference between the initial and optimal blades appears in the boundary layer separation zone on the suction side. In the former, the separation occupies almost all the suction sides except a small area near the blade tip. In the latter, the detachment zone is delayed with a percentage of 75%. When the TSR increases and reaches the value of 4, the flow field is fully attached on the optimized suction side and is developed with only slight separation occurring at the root and trailing edge. In fact, there are two main forces affecting the rotating blade and playing an important role in the boundary layer separation, the centrifugal forces that produce a span wise pumping effect that leads to the deviation of the streamlines in the span wise direction towards the tip. On the other hand, Coriolis forces, which act in the chord wise direction as a favorable pressure gradient tend to delay separation, Moreover, in all TSR values the highest-pressure levels can be observed along the leading edge of the pressure side from r=0.15m to r=0.3m. Meanwhile, on the suction side, the lowest pressure distribution on the suction side was observed at the leading edge between r=0.2m and r=0.3m. Therefore, the pressure difference between suction and pressure surfaces in the tip region is the first responsible generating the torque in the wind turbine and leads consequently to creating most of the power in this region.

6.4 Comparison Analysis Between BEM and CFD

In this section, a comparison is carried out between different values of the tip speed ratio of the micro wind turbine performance. The optimized curves for both methods show high values of power coefficient compared to the baseline configuration over the entire TSR range. The results between CFD and Qblade show a good agreement over operating range especially at design TSR

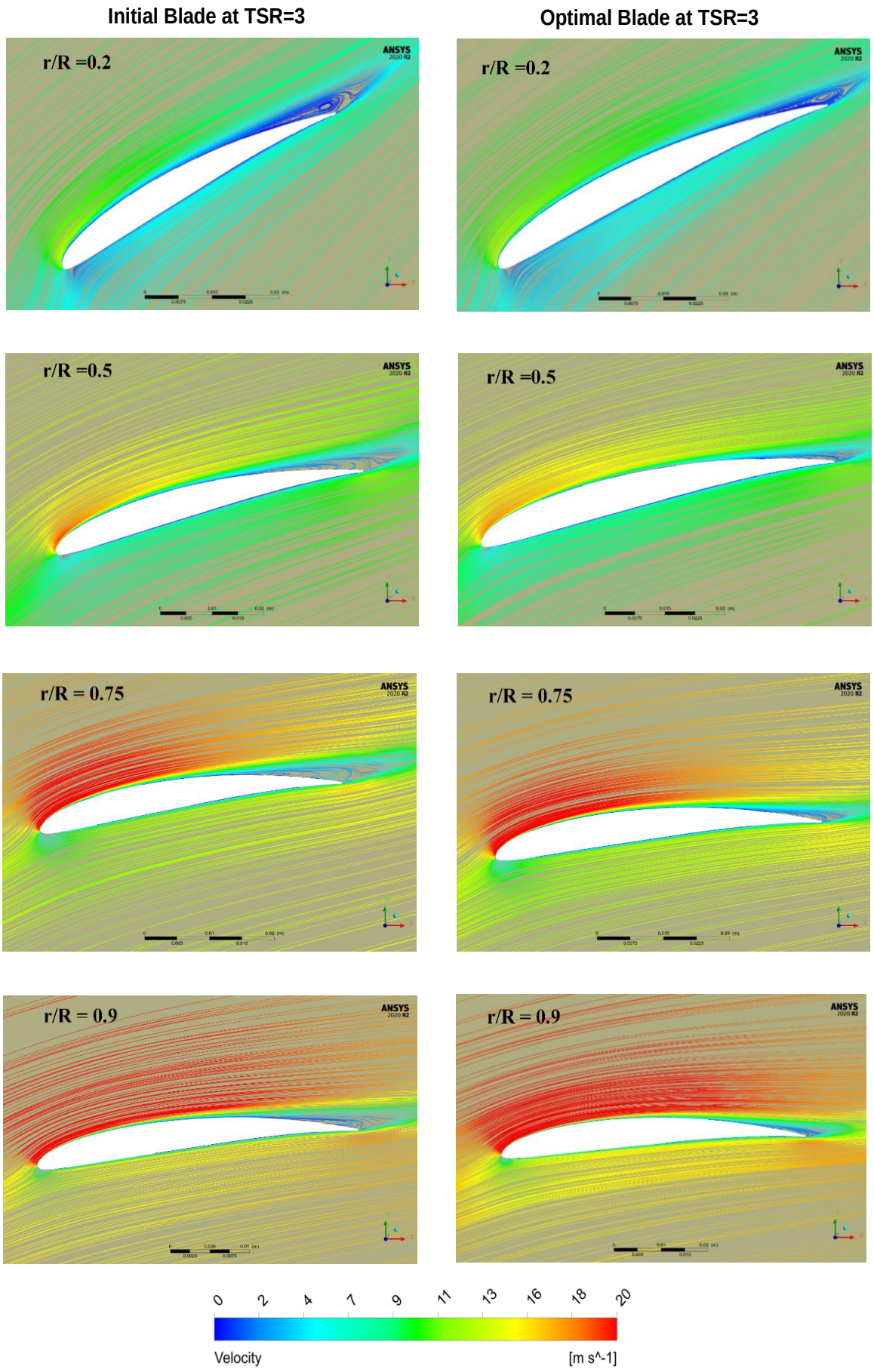

Fig. 17 Comparison the velocity streamlines between the initial and optimal blade at design TSR

Table 6 performance benefits of all TSR values

Tip speed ratio	Diff Cp in CFD between two wind turbine types	Diff Cp in Qblade between two wind turbine types
3	14.65%	17.17%
2.5	29.7%	32.41%
3.5	9.51%	27.2%
4	19.44%	41%
2	32%	56%

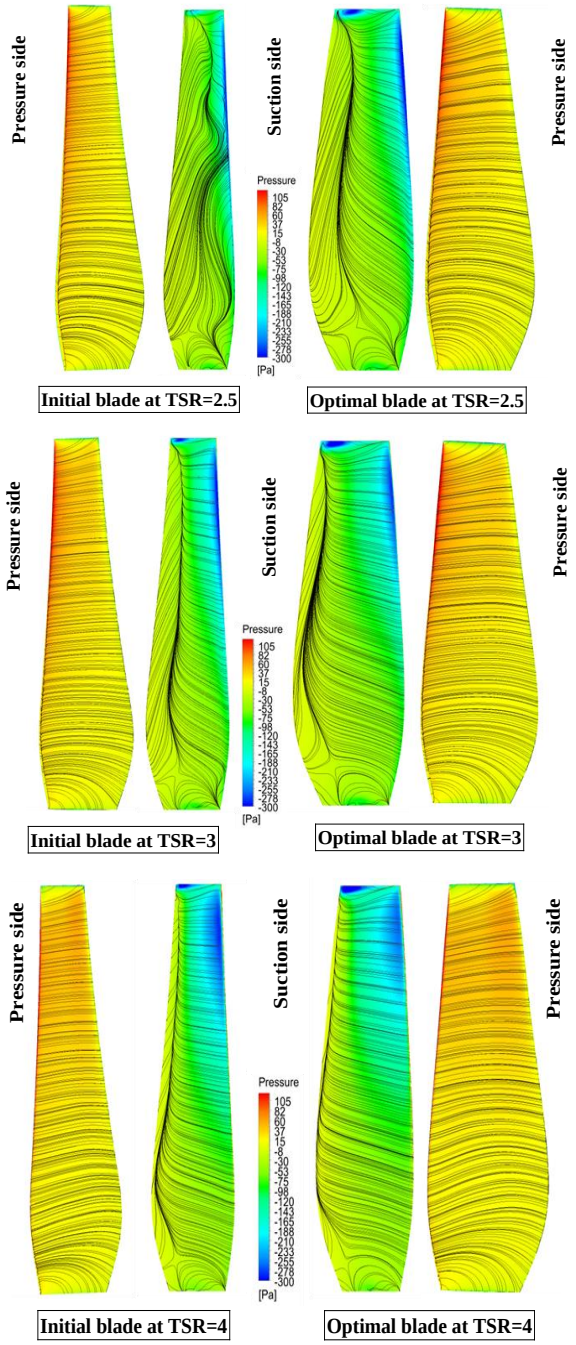

Fig. 18 limiting streamlines with static pressure contour of optimal and initial rotor at different tip speed ratio

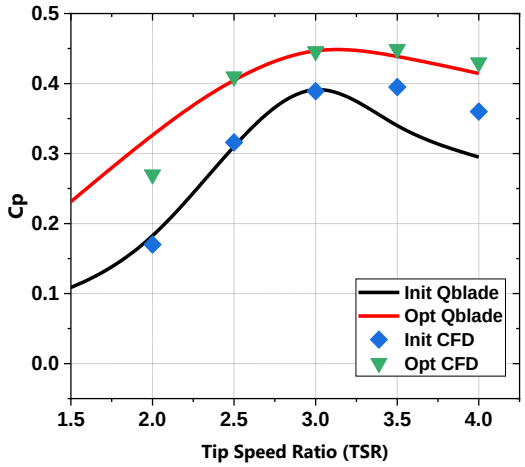

Fig. 19 Comparison between BEM and CFD

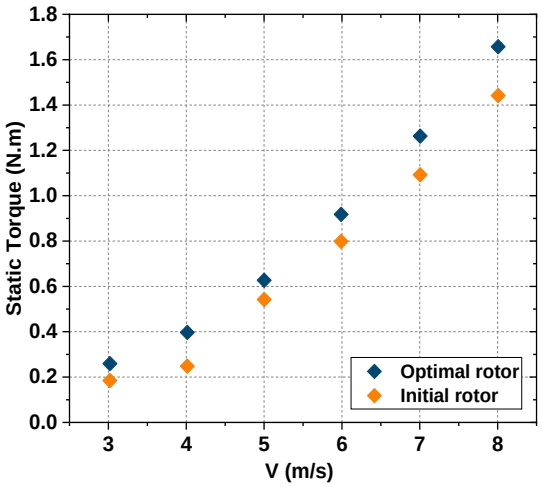

Fig. 20 Static torque at different wind speed for both rotors

and its neighboring except for the noticeable divergences, in the initial configuration between CFD and Qblade in the post-design region TSR>3 and in the optimized configuration between CFD and Qblade in the predesign region TSR<2.5. Table 6 shows the differences of the performance benefits between the two types of rotors at all TSRs. The reasons for these differences, are summarized in the following point; at high TSRs, where the rotational effects are considered in the CFD tool, the performance is increased compared to the Qblade results. On other hand, low TSRs, lead to the high angle of attack and consequently the separation of the boundary layer which deteriorate the wind turbine performance Fig. 19.

6.5 Torque Static Comparison

In this section, after selecting the design TSR=3 with five different speeds v=3,4,5,6,7 and 8 m/s, the static torque was examined using CFD tool for both initial and

optimal rotor, as shown in Fig. 20. In fact, the static torque rises with the increasing in wind speed for each rotor and the optimal rotor achieves highest torque values at all wind speeds. In particular, at the lowest speed v=3m/s, an increase of 37% was attained in the static torque for the optimal rotor compared to the initial one and this explains the enhancement in the starting-up ability during of the optimized turbine operability.

5. CONCLUSION

In this work the response surface method was used to optimize the aerodynamic geometry of the horizontal axis wind turbine blade based on the SG 6043 profile. In the first step, the BEM approach was utilized to give the preliminary design and analysis of the baseline configuration and was adopted as an initial geometry. This latter was identified by the chord length and twist angle distribution in the optimization process. A modelling geometry via both fourth degree and quadratic polynomial was applied to well-fitting curves over the full span for the chord length and twist angle distribution to minimize the sample points in the design of the experiment step. The non-parametric regression technique was added to the optimization process to build a high-quality response surface and the multi-objective genetic algorithm was implemented to identify the optimal objective function value. After a long time of calculation, the optimal blade was identified, and the results show through a comparison between the initial and optimized blade using the CFD analyzer and Qblade software that the performance of wind turbine increases by almost 14.65% and 17.17% at design TSR, respectively. The analysis of the flow topology near both blade sides illustrates that the benefit of the aerodynamic optimization revealed in the control of the detachment of the boundary layer especially at the trailing edge of the suction side. The adopted optimization process led to improve the starting operability in the lowest wind speed of V=3 m/s with almost 37%.

CONFLICT OF INTEREST

The authors state that they were unaware of competing financial interests and individual relationships that may affect the work demonstrated in this paper.

AUTHORS CONTRIBUTION

Bekkai Riyadh: Numerical investigation, programming, formal analysis and writing-original draft, writing-review & editing, methodology. **Mdouki Ramzi:** formal analysis and writing-original draft, writing-review & editing, methodology. **Laouar Roudouane:** formal analysis, supervision, and writing-review.

REFERENCES

Aelaei, M., Karimian, S., & Ommi, F. (2019). Sensitivity analysis and optimization of delta wing design parameters using CFD-based response surface method. *Journal of Applied Fluid Mechanics*, *12*(6), 1885-1903. https://doi.org/10.29252/JAFM.12.06.29706

Akhlaghi, M., Asadbeigi, M., & Ghafoorian, F. (2023). Novel CFD and DMST Dual method parametric study and optimization of a darrieus vertical axis wind turbine. *Journal of Applied Fluid Mechanics*, *17*(1), 205-218. https://doi.org/10.47176/JAFM.17.1.1985

ANSYS FLUENT User's Guide. ANSYS Inc, (2010).

Bai, C. J., Chen, P. W., & Wang, W. C. (2016). Aerodynamic design and analysis of a 10-kW horizontal-axis wind turbine for Tainan, Taiwan. *Clean Technologies and Environmental Policy*, *18*, 1151-1166. https://doi.org/10.1007/s10098-016-1109-z

Bekkai, R., Laouar, R., & Mdouki, R. (2024). Design optimization of three-dimensional geometry of a micro horizontal axis wind turbine blade using the response surface method. *PAMM*, e202300248. https://doi.org/10.1002/pamm.202300248

Benim, A. C., Diederich, M., & Pfeiffelmann, B. (2018). Aerodynamic optimization of airfoil profiles for small horizontal axis wind turbines. *Computation*, *6*(2), 34. https://doi.org/10.3390/computation6020034

Ceyhan, O., Sezer-Uzol, N., & Tuncer, I. (2009). *Optimization of horizontal axis wind turbines by using BEM theory and genetic algorithm.* Proceedings of the 5th Ankara International Aerospace Conference; METU: Ankara, Turkey. pp. 17–19. http://aiac.ae.metu.edu.tr/handle/11511/79495

Design Xplorer Documentation. ANSYS Inc, (2010).

Drela, M., & Aero, M. I. T. (2001). *Astro: XFOIL 6.94 User Guide*. Harold Youngren, Aerocraft.

Glauert, H. (1976). *Airplane Propellers. In Division L of Aerodynamic Theory*. Springer: Berlin/Heidelberg, Germany.

Hasan, M. M., El-Shahat, A., & Rahman, M. (2017). Performance investigation of three combined airfoils bladed small scale horizontal axis wind turbine by BEM and CFD analysis. *Journal of Power and Energy Engineering*, *5*(5), 1. https://doi.org/10.4236/jpee.2017.55002

Huang, B., Usui, Y., Takaki, K., & Kanemoto, T. (2016). Optimization of blade setting angles of a counter-rotating type horizontal-axis tidal turbine using response surface methodology and experimental validation. *International Journal of Energy Research*, *40*(5), 610-617. https://doi.org/10.1002/er.3383

Khaled, M., Ibrahim, M. M., Abdel Hamed, H. E., & AbdelGwad, A. F. (2019). Investigation of a small

horizontal–axis wind turbine performance with and without winglet. *Energy*, 115921. https:// https://doi.org/10.1016/j.energy.2019.115921

Kim, B., Kim, W., Bae, S., Park, J., & Kim, M. (2011). Aerodynamic design and performance analysis of multi-MW class wind turbine blade. *Journal of Mechanical Science and Technology*, *25*(8), 1995–2002. https://doi.org/10.1007/s12206-011-0521-x

Kim, B., Kim, W., Lee, S., Bae, S., & Lee, Y. (2013). Developement and verification of a performance based optimal design software for wind turbine blades. *Renewable Energy*, 54, 166-172. https://doi.org/10.1016/j.renene.2012.08.029

Koç, E., Gunel, O., & Yavuz, T. (2016). Mini-scaled horizontal axis wind turbine analysis by qblade and CFD. *International Journal of Energy Applications and Technologies*, *3*(2), 87-92. https://dergipark.org.tr/en/pub/ijeat/issue/28204/299500

Lanzafame, R., Mauro, S., & Messina, M. (2013). Wind turbine CFD modeling using a correlation-based transitional model. *Renewable Energy*, *52*, 31-39. https://doi.org/10.1016/j.renene.2012.10.007

Lee, S. L., & Shin, S. (2020). Wind turbine blade optimal design considering multi-parameters and response surface method. *Energies*, *13*(7), 1639. https://doi.org/10.3390/en13071639

Li, J. Y., Li, R., Gao, Y., & Huang, J. (2010). Aerodynamic optimization of wind turbine airfoils using response surface techniques. *Proceedings of the Institution of Mechanical Engineers, Part A: Journal of Power and Energy*, *224*(6), 827-838. https://doi.org/10.1243/09576509JPE888

Maindonald, J., & Braun, W. J. (2010) *Data analysis and graphics using R: An example-based approach.* 3rd ed. Cambridge University Press. https://doi.org/10.1017/CBO9781139194648

Marten, D., & Wendler, J. (2013). *Qblade guidelines*. Ver. 0.6, Technical University of (TU Berlin), Berlin, Germany.

Mauro, S., Lanzafame, R., & Messina, M. (2017). An insight into the rotational augmentation on HAWTs by means of CFD simulations-Part II: Post-processing and force analysis. *International Journal of Applied Engineering Research*, *12*(21), 10505-10529. https://www.ripublication.com/ijaer17/ijaerv12n21_06.pdf

Menter, F. R., Kuntz, M., & Langtry, R. (2003). Ten years of industrial experience with the SST turbulence model. *Turbulence, Heat, and Mass Transfer*, *4*(1), 625-632. https://www.researchgate.net/publication/228742295_Ten_years_of_industrial_experience_with_the_SST_turbulence_model

Pape, A. L., & Lecanu, J. (2004). 3D Navier–Stokes computations of a stall-regulated wind turbine. Wind Energy: *An International Journal for Progress and Applications in Wind Power Conversion Technology*, *7*(4), 309-324. https://doi.org/10.1002/we.129

Rajib Kanti Monda, L., Gayathri, R., & Mercy Shanthi, R. (2019, June). Performance exploration of mixed airfoil small scale horizontal axis wind turbine blade by QBLADE and CFD - *International Journal of Recent Technology and Engineering*, 8 (1S4). https://www.ijrte.org/wp-content/uploads/papers/v8i1s4/A10600681S419.pdf

Reddy, S. R., Dulikravich, G. S., Sobieczky, H., & Gonzalez, M. (2019). Bladelets—Winglets on blades of wind turbines: A multiobjective design optimization study. *Journal of Solar Energy Engineering*, *141*(6), 061003. https://doi.org/10.1115/1.4043657

Sessarego, M., Feng, J., Ramos-García, N., & Horcas, S. G. (2020). Design optimization of a curved wind turbine blade using neural networks and an aero-elastic vortex method under turbulent inflow. *Renewable Energy*, *146*, 1524-1535. https://doi.org/10.1016/j.renene.2019.07.046

Shin, P., & Kim, K. (2020). *Aerodynamic performance prediction of SG6043 airfoil for a horizontal-axis small wind turbine.* Journal of Physics: Conference Series (Vol. 1452, No. 1, p. 012018). IOP Publishing. https://doi.org/10.1088/1742-6596/1452/1/012018

Sørensen, J. N. (2016). *General momentum theory for horizontal axis wind turbines* (Vol. 4). New York: Springer.

Sun, H. (2011). Wind turbine airfoil design using response surface method. *Journal of Mechanical Science and Technology*, *25*, 1335-1340. https://doi.org/10.1007/s12206-011-0310-6

Tabatabaeikia, S., Ghazali, N. N. B. N., Chong, W. T., Shahizare, B., Izadyar, N., Esmaeilzadeh, A., & Fazlizan, A. (2016). Computational and experimental optimization of the exhaust air energy recovery wind turbine generator. *Energy Conversion and Management*, *126*, 862-874. https://doi.org/10.1016/j.enconman.2016.08.039

Taghinezhad, J., Alimardani, R., Masdari, M., & Mahmoodi, E. (2021). Performance optimization of a dual-rotor ducted wind turbine by using response surface method. *Energy Conversion and Management*: *X*, *12*, 100120. https://doi.org/10.1016/j.ecmx.2021.100120

Tahani, M., & Moradi, M. (2016). Aerodynamic investigation of a wind turbine using CFD and modified BEM methods. *Journal of Applied Fluid Mechanics*, *9*(1), 107-111. https://doi.org/10.36884/JAFM.9.SI1.25820

Yang, Y., Xue, Y., Zhao, W., Yang, H., & Wu, C. (2024a). Aerodynamic shape optimization based on proper orthogonal decomposition reparameterization under small training sets. *Aerospace Science and Technology*, *147*, 109072. https://doi.org/10.1016/j.ast.2024.109072

Yang, Y., Xue, Y., Zhao, W., Yao, S., Li, C., & Wu, C. (2024b). Fast flow field prediction of three-dimensional hypersonic vehicles using an improved Gaussian process regression algorithm. *Physics of Fluids*, *36*(1). https://doi.org/10.1063/5.0183291

Yang, Y., Zhao, W., Xue, Y., Yang, H., & Wu, C. (2023). Improved automatic kernel construction for Gaussian process regression in small sample learning for predicting lift body aerodynamic performance. *Physics of Fluids*, *35*(6). https://doi.org/10.1063/5.0153970

Zach, B. (2021). Curve Fitting in Excel, https://www.statology.org/curve-fitting-in-excel/

Zhou, L., Wang, Z., & Shi, J. (2020). Optimization design of the integral inertial particle separator based on response surface method. *Journal of Applied Fluid Mechanics*, *13*(1), 133-145. https://doi.org/10.29252/JAFM.13.01.30186